Integrating Materials and Manufacturing Innovation
https://doi.org/10.1007/s40192-019-00136-5

THEMATIC SECTION: 3D MATERIALS SCIENCE

A Tool to Generate Grain-Resolved Open-Cell Metal Foam Models

Joseph C. Tucker[1] · Ashley D. Spear[2]

Received: 1 March 2019 / Accepted: 25 April 2019

Abstract
The development and use cases of an open-source filter for DREAM.3D that instantiates synthetic, grain-resolved, open-cell metal foam volumes are presented. The new capability allows for both synthetic-grain overlay of X-ray computed tomography data as well as fully synthetic foam geometry and grains. For the latter, a novel technique using Euclidean distances instantiates the 3D open-cell foam morphology, enabling user control of pore size, strut cross-section shape, and strut thickness variability. By integrating this approach into the DREAM.3D architecture, the entire DREAM.3D suite of filters is immediately available; thus, enabling both user control and quantification of grain size, shape, and crystallographic orientation statistics (among other metrics) as well as meshing algorithms to enable subsequent numerical analysis.

Keywords Metallic foam · Cellular solid · Porous metals · Microstructure · Simulation

Introduction

Open-cell metal foams—including stochastic foams and lattice structures—are structural-material systems comprised of interconnected ligaments (referred to herein as struts) forming a hierarchical structure that includes the scales of the sub-strut (e.g., grain structure), strut, cell, and bulk foam. The reported relative density (or equivalently, volume fraction) of open-cell metal foams can range from 1% upwards to approximately 40%, depending upon the manufacturing technique used to produce the foam [1]. Due to their open-cell porous structure and ultra-low density, these structural materials have been used in a wide variety of multi-functional applications [2–4]. For example, in addition to serving as light-weight, load-bearing structures, open-cell metal foams can serve concurrently as electrodes for energy-storage devices [5], as hosts for newly generated bone and blood vessels in biomedical implants [6–8], or as impact absorbers and noise insulators for advanced high-speed ground transportation [4], to name a few.

✉ Joseph C. Tucker
jtucker@exponent.com

[1] Exponent, Inc, 149 Commonwealth Drive, Menlo Park, CA 94025, USA

[2] Department of Mechanical Engineering, University of Utah, Salt Lake City, UT 84112, USA

There have been many efforts in the literature to model open-cell metal foams to enable prediction of their mechanical (e.g., [9, 10]) and thermal-fluid (e.g., [11–13]) properties. Techniques for generating 3D models of open-cell metal foams can be classified into two general categories: (1) conversion of real data from, e.g., X-ray computed tomography ("CT") measurements [9, 14–20] and (2) generation of synthetic foams to represent both periodic unit-cell structures and stochastic foams. In the second case, the most common geometries used in modeling periodic unit-cell foams are the tetrakaidecahedron (or Kelvin's cell, e.g., [10]) and the Weaire-Phelan cell [21], which have been compared quantitatively to the geometrical features in stochastic foams [22]. To model stochastic foams, researchers have implemented a variety of techniques, including the application of Voronoi tessellations [12, 23] and spherical packing followed by Voronoi decomposition [24], which have resulted in very realistic foam structures. Surface evolver [25] is a software that can be used to generate realistic foam structures based on energy minimization reminiscent of the foaming process and has been used by a number of researchers to generate stochastic-foam models [13, 26, 27]. A relatively recent software, called GeoDict, has a FoamGeo module that allows for generation of both periodic unit-cell and stochastic foam structures and has been used by a number of researchers (e.g., [28]).

Despite the growing interest in modeling open-cell metal foams, all of the modeling efforts described above have resolved the foams to the cell level, treating each strut as a

Published online: 04 June 2019

material continuum. In fact, to the authors' knowledge, there have been no modeling efforts of open-cell metal foams that incorporate grain structure. Nonetheless, some experimental studies have suggested that grain structure could play an important role in determining the mechanical response of open-cell foams. For example, work by Goussery et al. [29] found that the yield strength of non-oxidized samples of open-cell, hollow-strut nickel foam decreased with increasing grain size up to the thickness of the strut wall. Additionally, Plumb et al. [30] recently mapped the 3D grain structure of open-cell aluminum foam and found that grain sizes were on the order of the size of the strut, suggesting that size effects due to grain structure could influence mechanical response of the foams.

In light of the above motivation, the aim of this paper is to describe a recent software development that enables generation of realistic open-cell foam models that are resolved to the scale of individual grains. The new capability has been implemented as a filter within the widely used, open-source software DREAM.3D [31]. Whereas, DREAM.3D conventionally enables instantiation of fully-dense, multi-phase material microstructures, the new filter now enables instantiation of open-cell polycrystalline foams. The foam geometry at the cell level can either be fully synthetic or based on CT data (on which grain structure is overlaid). The filter (and by extension, DREAM.3D) allows user control over pore size, strut cross-section shape, strut thickness and thickness variability, grain size, and crystallographic texture, among other attributes. The filter provides a new and powerful tool to investigate performance of open-cell polycrystalline foams by accounting for the hierarchical structure of the foam down to the grain scale.

Methods

A filter for DREAM.3D has been developed to instantiate the open-cell foam models in this study [31]. There are two distinct routes by which the grain-resolved open-cell foam structure can be instantiated: (1) Grain Overlay of CT Data and (2) Fully Synthetic Foam Volumes. These are both detailed below.

Grain Overlay of X-Ray Computed Tomography Data

For this approach, CT data are input into DREAM.3D and a synthetic grain structure is overlaid; thus, producing a grain-resolved open-cell foam model. To demonstrate, a text file of a CT scan from previous experimental measurements by Plumb et al. [30] is used here (FoamVoxel.txt). The reader is referred to [30] for details regarding acquisition of the experimental CT data. The nominal domain size is 200^3 voxels with a resolution of 0.0258, 0.02745, and 0.02355 mm in x, y, and z, respectively. The high-level workflow for the grain overlay of CT data in DREAM.3D is:

1. Read in CT data "mask"
2. Generate grain goal statistics
3. Pack grains and apply the mask
4. Calculate output statistics (e.g., grain size, shape, etc.)
5. Output structure and statistics

Fully Synthetic Foam Volumes

For this approach, input statistics are generated for both pore and grain phase in DREAM.3D. The main difference here is that input statistics are generated to define and instantiate the foam morphology, as opposed to that information being provided via input of CT data in the previously described approach. The high-level workflow for the fully synthetic foam volumes in DREAM.3D is:

1. Generate pore and grain goal statistics
2. Establish foam morphology (based on pore goal statistics)
3. Pack grains and apply the foam morphology "mask"
4. Calculate output statistics (e.g., grain size, shape, etc.)
5. Output structure and statistics

Euclidean Distance Maps to Generate Foam Morphology

For Step 2 in the above Fully Synthetic Foam Volume DREAM.3D workflow (i.e., establish foam morphology), a novel technique is used that leverages Euclidean distances. Three different Euclidean distances are calculated in DREAM.3D:

1. Boundary Euclidean distance: each voxel's distance to its nearest boundary
2. Triple Line Euclidean distance: each voxel's distance to its nearest triple line
3. Quadruple Point Euclidean distance: each voxel's distance to its nearest quadruple point (or higher coordination point)

In this case, boundaries, triple lines, and quad points are in terms of pores (e.g., a triple line is the intersection of three pores).

Figure 1[1] shows the three aspects of open-cell, grain-resolved, metal foam morphology represented by Euclidean distances, or quantities thereof. Note the series of images in Fig. 1 is for demonstrative purposes only. The various user inputs to produce the structure are not detailed. Figure 1a is a generic single-phase polycrystal instantiated with DREAM.3D. Figure 1b is the same as Fig. 1a, but with a Triple Line

[1] All DREAM.3D instantiation images in this paper were taken in ParaView.

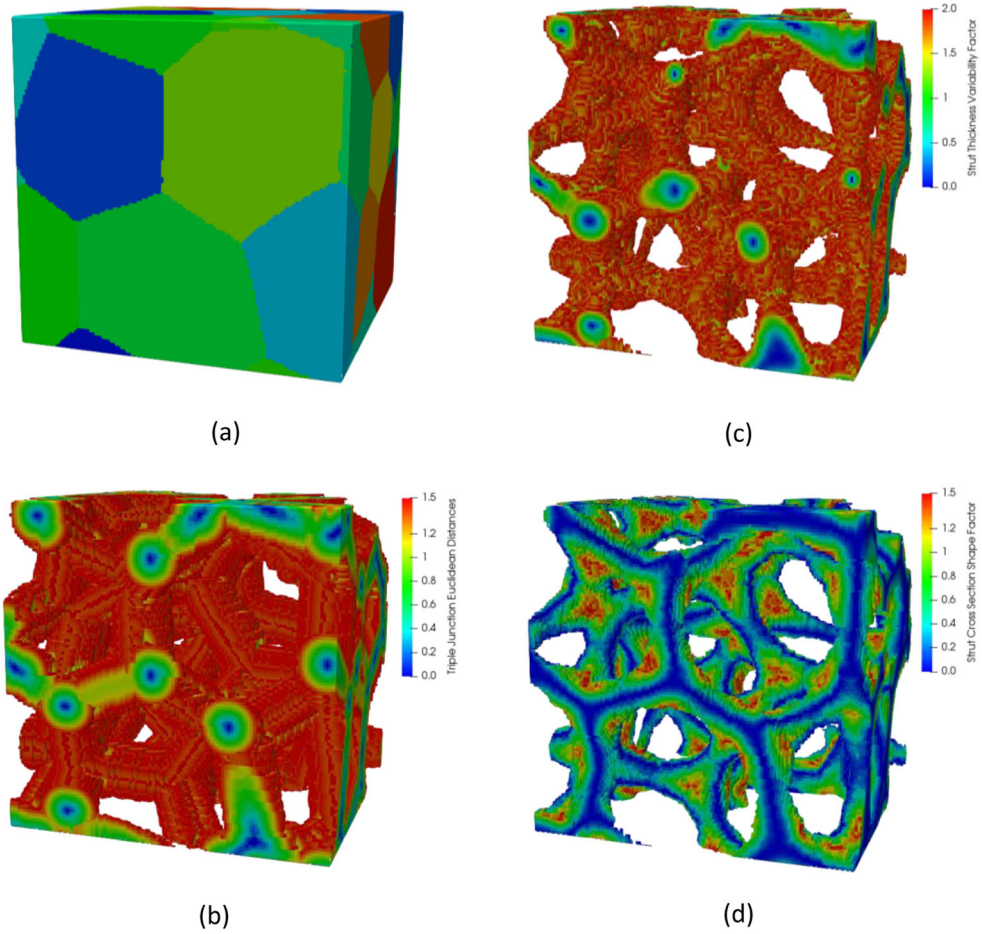

Fig. 1 **a** Generic single-phase polycrystal instantiated using DREAM.3D **b** Instantiation **a** with a Triple Line Euclidean Distance Threshold = 1.5 scaled units **c** Instantiation **a** with a Strut Thickness Variability Factor threshold = 2 scaled units[2]. **d** Threshold instantiation **c** with a Strut Cross-section Shape Factor threshold = 1.5 scaled units[2]. Note that the DREAM.3D-instantiated structure was scaled such that the voxels do not directly correspond to the thresholds

Euclidean distance threshold applied. The dilated triple line network, as defined by the threshold, effectively becomes the open-cell strut network.

There are two characteristics of open-cell foam morphology that Euclidean distances capture in this work. The first is strut-thickness variability, i.e., that struts tend to be thicker towards the node and thinner towards strut midpoint away from the node. This is captured in the below equation for Strut Thickness Variability Factor, which is the product of Triple Line Euclidean distance and Quadruple Point Euclidean distance. With this factor, more voxels will satisfy a given strut thickness variability factor threshold near the quadruple point, i.e., strut network node; thus, being represented as thicker. Concurrently, voxels further away from the node, yet remaining relatively close to the triple line, will also satisfy the threshold. The result is the characteristic concave isosurface (i.e., gravity well-type surface) moving away from (or towards) the nodes, as shown in Fig. 1c.

The second characteristic of open-cell foams captured via Euclidean distances is the strut cross section shape, i.e., that strut cross section shape ranges from near-circular, to a circular triangle or Reuleaux triangle (i.e., a triangle with convex edges), to a pseudotriangle (i.e., a triangle with concave edges). This shape is determined by the relative density and pores per unit volume [32]. This morphology emerges from the interaction/surface energy of the pores with each other. This surface shape is captured, in part,[2] in the below equation for Strut Cross Section Shape Factor, which is the product of Triple Line Euclidean distance and Boundary Euclidean distance. With this factor, for voxels along a given triple line, i.e., strut, those closer to a boundary (i.e., interface between two pores) will satisfy the criterion as opposed to other voxels at the same distance from a triple line but further away from a pore interface. The result is shown in Fig. 1d. The aforementioned characteristic triangle variations depend on the threshold that is set.

Figure 2 shows a pseudocode for implementation of the establish foam morphology filter in DREAM.3D. Note that the minimum Triple Line Euclidean distance is included so that the struts are enforced to remain connected. This overrides the other user inputs in the filter. Also note that all factors are effectively applied simultaneously in a compound conditional. The reader is referred to the DREAM.3D documentation for additional

[2] The Strut Cross Section Shape Factor only functions as the (set theory) intersection (i.e., ∩) with the Strut Thickness Variability Factor. The Strut Thickness Variability Factor functions independently.

```
all_cells == OFF
for (all_cells)
{
        F_thickness[cur_cell] = d_TL[cur_cell] * d_QP[cur_cell]
        F_shape[cur_cell] = d_TL[cur_cell] * d_B[cur_cell]
        if (
        d_B[cur_cell] < d_B_min_thres
        &&
        F_thickness[cur_cell] < F_thickness_thres
        &&
        F_shape[cur_cell] < F_shape_thres
        )
        {
                cur_cell == ON
        }
}
```

Fig. 2 Pseudocode for the establish foam morphology filter implemented in DREAM.3D

information regarding the "Find Euclidean Distance Map" and "Establish Foam Morphology" filters and their usage.

Strut thickness variability factor $= d_{TL}d_{QP}$; and,
Strut Cross section shape factor $= d_{TL}d_B$; where,
d_{TL} = Triple Line Euclidean Distance;
d_{QP} = Quadruple Point Euclidean Distance; and,
d_B = Boundary Euclidean Distance

Results

CT with Grain Overlay

This section presents the CT data, as described in the "Methods" section, in two variations: (1) overlay with a relatively large grain size and (2) overlay with a relatively small grain size. While the example presented here relies on CT data to establish the foam morphology, it is emphasized that the actual source of the foam morphology used in the grain-overlay approach is not limited to CT-derived data. For example, a user could generate a foam structure using another methodology (e.g., GeoDict/FoamGeo or Surface Evolver) and, provided the data can be expressed in an analogous format, overlay a synthetic grain structure.

Larger Grain Size

The procedure for generating the structure shown in Fig. 3 is detailed in the "Grain Overlay of X-Ray Computed Tomography Data" Section. The DREAM.3D pipeline file used to instantiate the model shown in Fig. 3 is "CT_large_grains_1-25-19.json" and has been provided. The relevant input parameter that controls grain size is the lognormal mean grain size. This parameter was set to 0.1, which corresponds to an equivalent-sphere-diameter grain size of approximately 1.105. The resulting instantiation has 119 grains.

Smaller Grain Size

The procedure for generating the structure shown in Fig. 4 is the same as the larger grain size instantiation. The DREAM.3D pipeline file used to instantiate the model shown in Fig. 4 is "CT_small_grains_1-28-19.json" and has been provided. The lognormal mean, as with the larger grain size instantiation, was set to 0.1. However, the resolution in x, y, and z were all 4 times multiplied resulting in 0.1032, 0.1098, and 0.0942 "scaled mm," respectively.[3] This effectively decreased the average grain volume by 4^3 (i.e, 64 times). The resulting instantiation has 2067 grains.

Comparison of Grain Size Instantiations with Goal Statistics

Looking at how well the goal grain size was met, it must be considered that the vast majority of grains are surface grains, i.e., in some degree of contact with the foam boundary. Thus, it was not expected that the actual grain size distribution would be representative of the goal grain size distribution. In fact, all 119 grains in the smaller grain size instantiation and all but five of the 2067 grains in the larger grain size instantiation are surface grains; therefore, almost every grain is biased to varying degrees. Given the morphology of open-celled foams versus fully-dense polycrystals (i.e., significantly higher surface-area-to-volume ratio), a reasonable workaround with a fully-dense polycrystal (i.e., remove the biased [33] and/or surface grains from the analysis or use periodic boundary conditions) is not an option. However, one way to account for the bias would be to shift the input grain size mean (and potentially standard deviation) in StatsGenerator.

[3] Note that the use of "Change Scaling of Volume" is only needed because the native CT scan resolution was small such that the minimum of a lognormal mean did not allow to make the grain size smaller through a more straightforward route. As a workaround, the scaling was defined as ¼ the native scan resolution; the grains are then packed, and the resolution is subsequently changed to the native CT scan resolution. In similar studies with larger scan resolution, the user should simply change the mean in StatsGenerator.

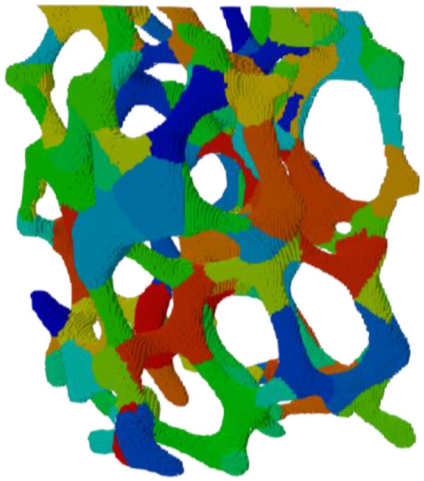

Fig. 3 DREAM.3D instantiation of CT data with "larger" grain synthetic overlay. The grains are colored by arbitrary identification

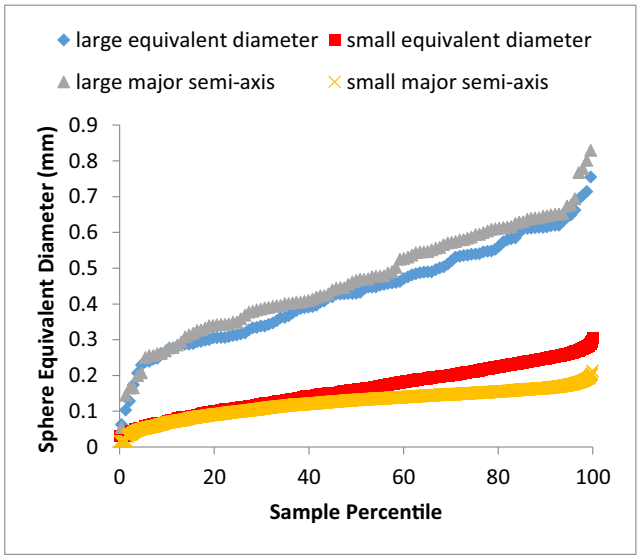

Fig. 5 Lognormal probability plot of equivalent diameter and major semi-axis length for the larger grain size instantiation (blue) and smaller grain size instantiation (gray) with the same open-cell foam morphology instantiation. Due to the 4 times scaling applied to the voxel sizes (as described in the text), the smaller grain size instantiation grain sizes were multiplied by 4 to equate the scaling between the two instantiations

Another potential way to deal with the bias would be to apply a minimum grain size threshold after the structure is instantiated.

To further analyze the degree of shift in actual versus goal grain size and also examine grain shape, Fig. 5 shows a lognormal probability plot of sphere-equivalent grain sizes and ellipsoid-fit major semi-axis lengths for the smaller and larger grain instantiations. The larger grain size instantiation distribution shows heavy lower tail departure, i.e., there are more small grains than what a lognormal distribution would predict. All distributions show a light upper tail departure, i.e., there are fewer large grains than what a lognormal distribution would predict. The larger grain size instantiation major semi-axis lengths are consistently larger than the larger grain size instantiation equivalent diameters throughout the distribution and both distributions exhibit a similar probability plot shape. The smaller grain size instantiation exhibits an opposite trend, with the major semi-axis lengths smaller than the equivalent diameters, especially in the mean field and increasingly more so in the upper tail of the distribution. This result is perhaps not as intuitive; however, the ellipsoid-fit for smaller grain sizes may be not as representative as for larger sizes as individual voxel geometry (i.e., corners and edges), will more heavily influence the ellipsoid-fit. Just as with the smaller grain size instantiation, both the major semi-axis length and equivalent diameter probability plot exhibit a similar shape. For reference, the goal equivalent grain size distribution should be a monodisperse distribution around 1.105. A "goal grain" is an ellipsoid, generated from the lognormal input statistics, used in the packing algorithm in the DREAM.3D Pack Primary Phases Filter. More information on the packing algorithm is available in Tucker et al. [34]. Equivalent sphere diameter is used primarily as a measure of volume in this work. However, further quantifying shape beyond ellipsoid-fit aspect ratio and major semi-axis length may be useful for further studies. Metrics such as degree of biasing (i.e., percent of voxels that touch the surface), surface area to volume ratio, and roughness (tightest fitting convex hull over area) may be considered.

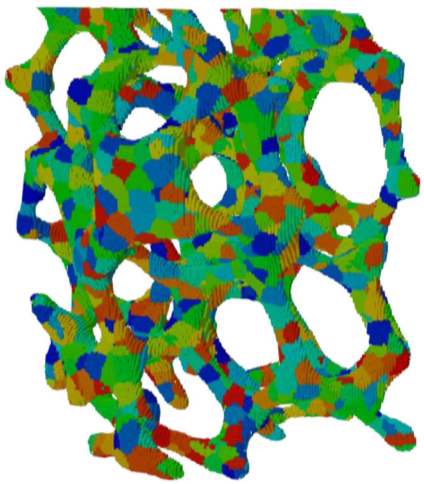

Fig. 4 DREAM.3D Instantiation of CT data with "smaller" grain size synthetic overlay. The grains are colored by arbitrary identification

A selection of statistics for the smaller and larger grain size instantiations are shown in Table 1. Further grain distribution attributes (e.g., shape and neighborhood) may also be calculated in DREAM.3D if those attributes are determined to be important for subsequent studies (e.g., numerical simulation).

The authors note that the grain-packing algorithm is independent of the morphology of the foam. The implication is that the current framework cannot capture grain-size variation induced by geometrical constraints imposed during the solidification process, as an example. A non-trivial extension to the current framework would be to include a more physics-driven grain-growth

model that accounts for the foam morphology, which is beyond the scope of the current work.

Fully Synthetic

This section presents the instantiation results of fully synthetic, grain-resolved, open-cell foam, as described in the "Methods" Section, and demonstrates user control of four features: (1) pore size, (2) strut thickness variability, (3) strut cross-section shape, and (4) pore aspect ratio. The procedure for generating the structures shown in this section are detailed in the "Fully Synthetic Foam Volumes" and "Euclidean Distance Maps to Generate Foam Morphology" Sections. Note that all synthetic structures in this study are generated with a random crystallographic texture. Additionally, arbitrary units are used for the fully synthetic cases. These units may be defined and scaled however the user chooses, to suit specific needs. Similar to the case of CT foam with grain overlay, the grain-packing algorithm is independent of the foam morphology in the fully synthetic case, and future work could consider a coupled, physics-driven, grain-growth model.

Pore Size

The DREAM.3D pipeline file used to instantiate the model shown in Fig. 6a[4] is "small_pore_1–29-19.json" and the pipeline file used to instantiate the model shown in Fig. 6b is "large_pore_1-29-19." Both of these files have been provided. The relevant input parameter that controls pore size is the log-normal mean grain size for the pore phase in the StatsGenerator Filter. In the current implementation, the pores are defined as a precipitate phase in DREAM.3D, as it was the phase type that most closely satisfied the needs in the establish foam morphology filter. Future DREAM.3D versions could add a new phase type. This parameter was set to 4.50 and 4.75 for the small and large pore cases, respectively. The goal average equivalent-sphere diameter was approximately 90 and 116 units for the small and large pore case, respectively. The resulting instantiations have a mean sphere equivalent diameter pore size of 79 and 105 for the small and large pore case, respectively, with no surface or biased pores removed.[5] The purpose of this study was not to match the actual and goal statistics, but rather to illustrate that the pore size can be controlled in DREAM.3D.

[4] The ParaView clip utility is used to take an interior subset volume, because if non-periodic boundary conditions are used, then the Euclidean distances do not produce representative morphology near the domain boundary.

[5] Anecdotally, a good way to determine the Strut Thickness Variability Factor and Strut Cross Section Shape Factor is to set the "StatsGenerator" parameters and "Initialize Synthetic Volume" parameters, then run the pipeline with the defaults in "Establish Foam Morpholoy." Open the result in ParaView, then use the calculator utility to calculate Strut Thickness Variability Factor and Strut Cross Section Shape Factor (equations provided in the Euclidean Distance Maps to Generate Foam Morphology Section). Then use the Threshold Utility to determine what threshold satisfies the requirement, and use those thresholds as inputs in "Establish Foam Morphology."

Table 1 Selected statistics for the smaller and larger grain size instantiations

Instantiation	Larger grain size	Smaller grain size
Number of grains	119	2067
Number of surface grains	119	2062
Actual mean grain size equivalent sphere diameter	0.433 mm	0.160 mm
Goal mean grain size equivalent sphere diameter	1.104 mm	0.276 mm

Strut Thickness Variability

Figure 7a was run with the same input parameters as Fig. 6a, except the strut thickness variability factor was set to 100 instead of 250. The pipeline to generate the volume with a strut thickness variability factor of 100 is "low_variability_strut_1-30-19.json"

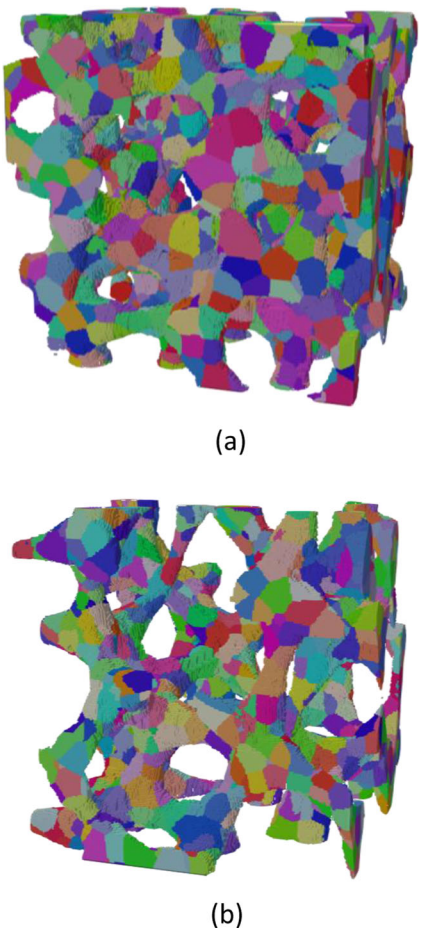

Fig. 6 DREAM.3D instantiations of fully-synthetic open-cell foam volumes with **a** smaller pores (lognormal mean = 4.5) and relative density of 31.2% and **b** larger pores (lognormal mean = 4.75) and relative density of 17.4%. The colors are mapped using inverse pole figure coloring with reference direction [001]. Refer to the DREAM.3D User Manual "Generate IPF Colors" page for more information

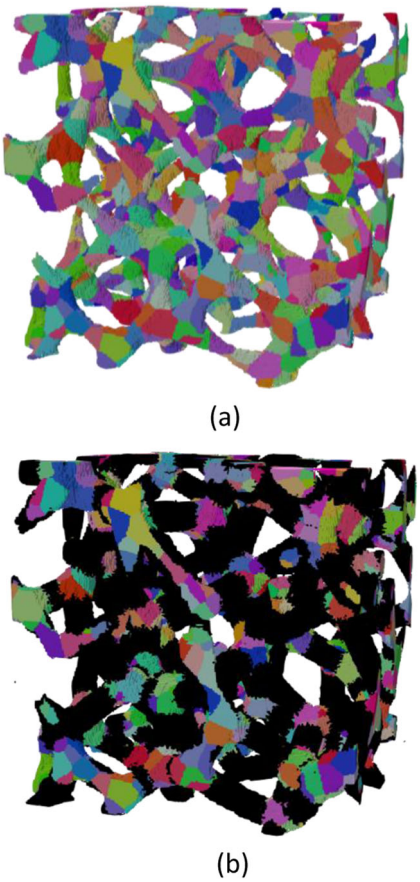

Fig. 7 DREAM.3D instantiation of a higher variability strut thickness open-cell foam with relative density of 11.8% and **b** lower variability strut thickness open-cell foam with relative density of 16.6%. The colors are mapped using inverse pole figure coloring with reference direction [001]. Refer to the DREAM.3D User Manual "Generate IPF Colors" page for more information. Both **a** and **b** are from the same instantiation, but the black cells in **b** are the result of a minimum strut thickness threshold of 8

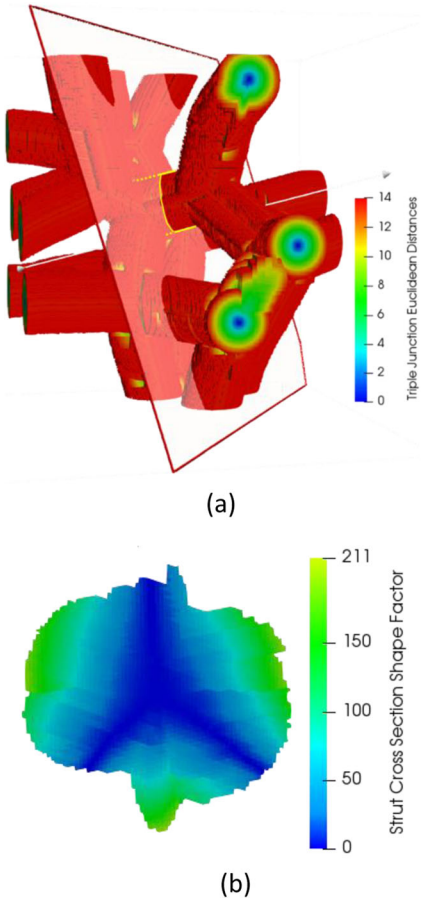

Fig. 8 DREAM.3D instantiation of **a** an open-cell foam with a minimum strut thickness threshold of 14 (scaled) with a cross section region of interest annotated with yellow markings **b** exposed slice from **a** colored by strut cross section shape factor

and is provided. Figure 7 series was produced by holding the strut thickness variability factor constant and changing the minimum strut thickness user input parameter (see Fig. 2). Figure 7b is the same instantiation as Fig. 7a except the added voxels from the minimum strut thickness threshold are colored black. The pipeline to generate the volume with a strut thickness variability factor of 100 and a minimum strut thickness of 8 is "low_variability_strut_1–30-19.json" and is provided. Different results may be obtained by holding the minimum strut thickness constant while varying the strut thickness variability factor, or even varying both.

Strut Cross-Section Shape

Figure 8 was instantiated with the same inputs as Fig. 6a, except the domain is 400^3 voxels and the scale is 0.4 in x, y, and z as opposed to a 300^3 voxel domain with an x, y, and z scale of 1.0. The increase in domain size coupled with the decrease in resolution was to further resolve the strut to more clearly show the cross-section shapes. Also, Fig. 7 is not showing the instantiation in its final form, but rather with the minimum triple line Euclidean distance threshold of 14 (similar to Fig. 1b). The minimum strut thickness threshold was 14 as opposed to 1, and the strut thickness variability and strut cross section shape factors were not enforced. Note that the instantiation shown in Fig. 8 is scaled differently than in Fig. 6a, so the thresholds are not a one-to-one comparison. The color map in Fig. 8b is scaled to embellish a low density foam (blue), medium density foam (blue+light blue), and a high density foam (entire cross section). Thus, given this input parameter set, enforcing a strut cross section shape factor in the range of 30, 80, and 150 would result in a low, medium, and high density foam cross section shape, respectively. For comparison, optical micrographs showing the variability in strut cross-section shapes of physical samples of open-cell aluminum foams are provided in Fig. 9. As indicated by the color gradation in Fig. 8b, the strut cross section shape factor enables a range of strut cross-section shapes that are consistent with those observed in real open-cell metal foams.

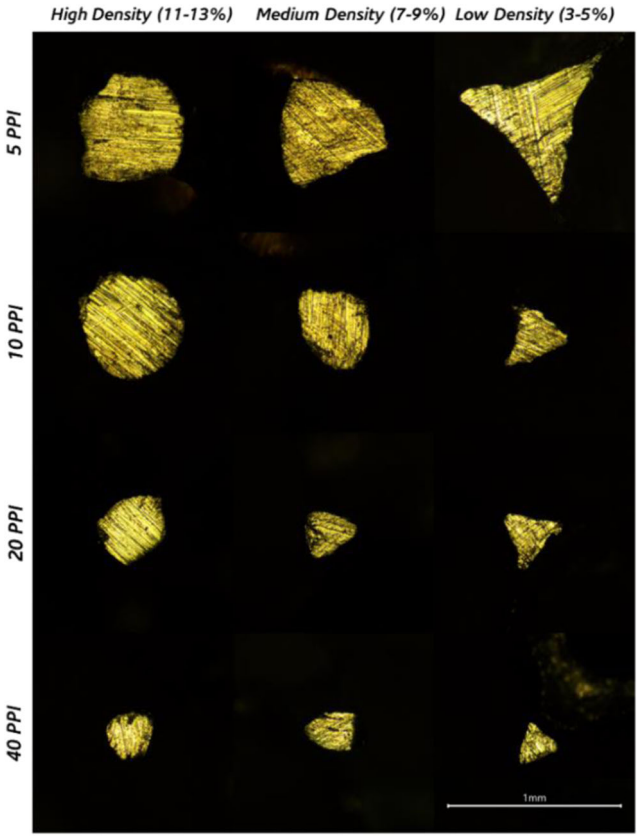

Fig. 9 Optical micrographs showing the variation in strut cross-section shapes and sizes for different combinations of pore sizes and densities of an open-cell aluminum foam (personal communication, unpublished)

Pore Aspect Ratio and Axis Orientation

It is common for real foam structures to exhibit some degree of preferential directionality leading to football-shaped cells. This feature can be captured by enforcing an aspect ratio in the DREAM.3D StatsGenerator Filter. A straightforward way to accomplish this is to use the Rolled Preset Statistical Model in Stats Generator. In Fig. 10, the rolled preset statistical model was used with an "A Axis Length" = 3.0. The "B Axis Length" and "C Axis Length" remain set to 1.0. The pipeline to generate the volume with a 3:1:1 goal aspect ratio is "pore_axis_1–30-19.json" and is provided. The result mean aspect ratio was 2.2:1.3:1; however, as can be seen from Fig. 10, the elongated pore axis is being cut off from the small domain size.[6] A larger domain would likely produce a result closer to the goal aspect ratio.

[6] Further, DREAM.3D does not distinguish between the sample direction and the larger and smaller minor semi-axis in terms of calculating aspect ratios. Instead, it simply rank orders them largest to smallest; therefore, the b:c aspect ratio of 1.3:1 may be closer to 1:1, which would further increase the major semi-axis aspect ratio component.

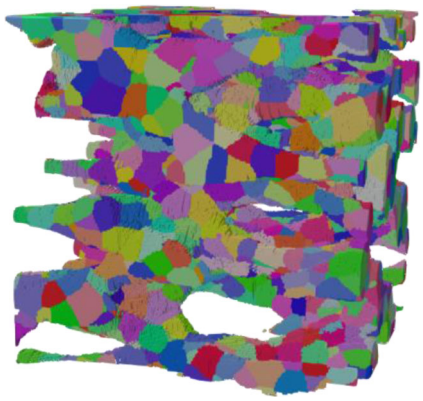

Fig. 10 DREAM.3D instantiation of an open-cell foam with a 3:1:1 pore aspect ratio and a relative density of 31.2%. The "3," i.e., x-axis direction is to the left and right of the page. The colors are mapped using inverse pole figure coloring with reference direction [001]. Refer to the DREAM.3D User Manual "Generate IPF Colors" page for more information

Accessibility and Required Computational Environment

A custom-built precompiled DREAM.3D version (DREAM3D-6.3.328.7b6444277-Win64) was used for this work, and a zip file is provided. The precompiled binary is compatible with Windows 64-bit systems. Users interact with the DREAM.3D graphical user interface (GUI) through a pipeline framework; i.e., filters that perform different tasks are layered in a sequential order, with each filter/task being executed in that order. The pipelines that produced many of the results in this study are cited and provided. The output files are not provided, as the DREAM.3D pipeline files will reproduce them (note, however, that some DREAM.3D filters that involve inherent randomness will not produce the exact output shown in this paper.) Only local system file paths need to be changed in the input and output files for the pipeline files to function properly. If a replacement input statistics file is not used, the "Create Data" button in the StatsGenerator filter needs to be clicked for each so that the statistics are properly initialized. Further information about the DREAM.3D data structure is available in Ref. [31]. DREAM.3D can be run on Mac, Windows, and Linux, from a basic laptop to a supercomputer (http://dream3d.bluequartz.net/). As previously mentioned, however, the DREAM.3D precompiled binary used and provided here is only compatible with Windows 64-bit systems.

Conclusions

An open-source filter for the open-source software DREAM.3D has been developed to enable instantiation of grain-resolved, open-cell, metal foam models. The new filter can be used to overlay synthetic grain structure on existing foam morphologies (e.g., from experimentally derived CT data), or to instantiate fully

synthetic open-cell foam morphologies and grain structure. The new filter is included in a pre-compiled version of DREAM.3D included with this paper. The main outcomes from this work are summarized as follows:

- The use of Euclidean distance maps to instantiate synthetic open-cell foam morphology allows users to control two characteristics observed in real foams.
  - Strut-thickness variability along the length of the strut, which can range from relatively uniform thickness to thicker towards the node and thinner towards the strut midpoint.
  - Strut cross-section shape, which can range from near-circular to triangular with convex edges to triangular with concave edges.
- A selection of the many options within DREAM.3D showed how users can vary pore size, pore aspect ratio (and axis orientation), and grain size.
- Due to the high surface-to-volume ratio of open-cell foams, many of the instantiated grains intersect free surfaces, resulting in a shift between the target and actual grain sizes. Adjusting the target grain-size distribution or applying size threshold merging are ways to account for this.
- Various use cases are presented to demonstrate the capability of the new establish foam morphology filter. The pipeline and input files used to produce results from the various use cases are provided with this paper.
- The new filter enables, for the first time, the incorporation of grain structure in open-cell metal foam models, thus facilitating an Integrated Computational Materials Engineering (ICME) [35] approach to the design of open-cell metal foams.

Funding Information This material is based upon work supported by the National Science Foundation DMREF program under Grant No. CMMI-1629660.

Compliance with Ethical Standards

Conflict of Interest On behalf of both authors, the corresponding author states that there is no conflict of interest.

References

1. Wadley HN (2002) Cellular metals manufacturing. Adv Eng Mater 4(10):726–733
2. Evans AG, Hutchinson J, Ashby M (1998) Multifunctionality of cellular metal systems. Prog Mater Sci 43(3):171–221
3. Banhart J (2001) Manufacture, characterisation and application of cellular metals and metal foams. Prog Mater Sci 46(6):559–632
4. Banhart J (2003) Aluminum foams: on the road to real applications. MRS Bull 28(04):290–295
5. Zhao C-Y, Lu W, Tian Y (2010) Heat transfer enhancement for thermal energy storage using metal foams embedded within phase change materials (PCMs). Sol Energy 84(8):1402–1412
6. Singh R, Lee P, Dashwood R, Lindley T (2010) Titanium foams for biomedical applications: a review. Mater Technol 25:127–136
7. Murr LE, Gaytan SM, Medina F, Lopez H, Martinez E, Machado BI, Hernandez DH, Martinez L, Lopez MI, Wicker RB, Bracke J (2010) Next-generation biomedical implants using additive manufacturing of complex, cellular and functional mesh arrays. Philos Trans R Soc Lond A 368(1917):1999–2032
8. Murr LE, Gaytan SM, Martinez E, Medina F, Wicker RB (2012) Next generation orthopaedic implants by additive manufacturing using electron beam melting. Int J Biomater 2012:1–14. https://doi.org/10.1155/2012/245727
9. Maire E, Fazekas A, Salvo L et al (2003) X-ray tomography applied to the characterization of cellular materials. Related finite element modeling problems. Compos Sci Technol 63(16):2431–2443. https://doi.org/10.1016/S0266-3538(03)00276-8
10. Jang WY, Kyriakides S (2009) On the crushing of aluminum open-cell foams: part II analysis. Int J Solids Struct 46(3–4):635–650. https://doi.org/10.1016/j.ijsolstr.2008.10.016
11. Krishnan S, Murthy JY, Garimella SV (2006) Direct simulation of transport in open-cell metal foam. ASME J Heat Transfer 128(8):793–799. https://doi.org/10.1115/1.2227038
12. Wehinger GD, Heitmann H, Kraume M (2016) An artificial structure modeler for 3D CFD simulations of catalytic foams. Chem Eng J 284(1385–8947):543–556. https://doi.org/10.1016/j.cej.2015.09.014
13. Das S, Sneijders S, Deen NG, Kuipers JAM (2018) Drag and heat transfer closures for realistic numerically generated random open-cell solid foams using an immersed boundary method. Chem Eng Sci 183(0009–2509):260–274. https://doi.org/10.1016/j.ces.2018.03.022
14. Zafari M, Panjepour M, Emami MD, Meratian M (2015) Microtomography-based numerical simulation of fluid flow and heat transfer in open cell metal foams. Appl Therm Eng 80:347–354
15. Della Torre A, Montenegro G, Tabor G, Wears M (2014) CFD characterization of flow regimes inside open cell foam substrates. Int J Heat Fluid Flow 50:72–82
16. Bianchi E, Heidig T, Visconti CG, Groppi G, Freund H, Tronconi E (2013) Heat transfer properties of metal foam supports for structured catalysts: wall heat transfer coefficient. Catal Today 216:121–134
17. Bianchi E, Heidig T, Visconti CG, Groppi G, Freund H, Tronconi E (2012) An appraisal of the heat transfer properties of metallic open-cell foams for strongly exo−/endo-thermic catalytic processes in tubular reactors. Chem Eng J 198:512–528
18. Ranut P, Nobile E, Mancini L (2014) High resolution microtomography-based CFD simulation of flow and heat transfer in aluminum metal foams. Appl Therm Eng 69(1):230–240
19. Iasiello M, Cunsolo S, Oliviero M, Harris WM, Bianco N, Chiu WK, Naso V (2014) Numerical analysis of heat transfer and pressure drop in metal foams for different morphological models. J Heat Transf 136(11):112601
20. Bodla KK, Murthy JY, Garimella SV (2010) Microtomography-based simulation of transport through open-cell metal foams. Numer Heat Transf Part A: Appl 58(7):527–544
21. Weaire D, Phelan R (1994) A counter-example to Kelvin's conjecture on minimal surfaces. Philos Mag Lett 69(2):107–110
22. Bock J, Jacobi AM (2013) Geometric classification of open-cell metal foams using X-ray micro-computed tomography. Mater Charact 75:35–43. https://doi.org/10.1016/j.matchar.2012.10.001
23. Siegkas P, Tagarielli V, Petrinic N (2014) Modelling stochastic foam geometries for FE simulations using 3D Voronoi cells. Procedia Mater Sci 4:221–226. https://doi.org/10.1016/j.mspro.2014.07.604

24. August A, Ettrich J, Rölle M, Schmid S, Berghoff M, Selzer M, Nestler B (2015) Prediction of heat conduction in open-cell foams via the diffuse interface representation of the phase-field method. Int J Heat Mass Transf 84:800–808
25. Brakke KA (1992) The surface evolver. Exp Math 1(2):141–165
26. Kopanidis A, Theodorakakos A, Gavaises E, Bouris D (2010) 3D numerical simulation of flow and conjugate heat transfer through a pore scale model of high porosity open cell metal foam. Int J Heat Mass Transf 53(11):2539–2550
27. Buffel B, Desplentere F, Bracke K, Verpoest I (2014) Modelling open cell foams based on the Weaire–Phelan unit cell with a minimal surface energy approach. Int J Solids Struct 51(19–20):3461–3470
28. Pabst W, Uhlířová T, Gregorová E, Wiegmann A (2018) Young's modulus and thermal conductivity of closed-cell, open-cell and inverse ceramic foams–model-based predictions, cross-property predictions and numerical calculations. J Eur Ceram Soc 38(6):2570–2578. https://doi.org/10.1016/j.jeurceramsoc.2018.01.019
29. Goussery V, Bienvenu Y, Forest S, Gourgues AF, Colin C, Bartout JD (2004) Grain size effects on the mechanical behavior of open-cell nickel foams. Adv Eng Mater 6(6):432–439. https://doi.org/10.1002/adem.200405153
30. Plumb JC, Lind JF, Tucker JC, Kelley R, Spear AD (2018) Three-dimensional grain mapping of open-cell metallic foam by integrating synthetic data with experimental data from high-energy x-ray diffraction microscopy. Mater Charact 144:448–460. https://doi.org/10.1016/j.matchar.2018.07.031
31. Groeber MA, Jackson MA (2014) DREAM.3D: a digital representation environment for the analysis of microstructure in 3D. Integr Mater Manuf Innov 3(1):5. https://doi.org/10.1186/2193-9772-3-5
32. Gibson LJ, Ashby MF (1999) Cellular solids: structure and properties (2nd ed). Cambridge, United Kingdom: Cambridge University Press
33. Rowenhorst DJ, Kuang JP, Thornton K, Voorhees PW (2006) Three-dimensional analysis of particle coarsening in high volume fraction solid-liquid mixtures. Acta Mater 54(8):2027–2039. https://doi.org/10.1016/j.actamat.2005.12.038
34. Tucker JC, Chan LH, Rohrer GS, Groeber MA, Rollett AD (2012) Tail departure of log-normal grain size distributions in synthetic three-dimensional microstructures. Metall Mater Trans A 43(8):2810–2822
35. Allison J, Backman D, Christodoulou L (2006) Integrated computational materials engineering: a new paradigm for the global materials profession. JOM 58(11):25–27